Multiconfiguration multichannel Schwinger study of the C(1s) photoionization of CO including shake-up satellites

Gunadya Bandarage and Robert R. Lucchese
Department of Chemistry, Texas A&M University, College Station, Texas 77843-3255
(Received 28 August 1992)

Often the inclusion of electron-correlation effects in photoionization calculations is crucial; e.g., calculation of satellite cross sections and asymmetry parameters in core ionization of molecules. We have developed a computational approach to include the relaxation, multiconfiguration, and multichannel effects, in a multichannel configuration-interaction (MCCI) approximation, for the study of molecular photoionization. Results are presented of a detailed MCCI-Schwinger study of the C(1s) core-hole production in CO, including the formation of the lowest two $\pi \rightarrow \pi^*$ shake-up satellites. It is shown that the multichannel effects are more important in describing the satellites than the core-hole channel.

PACS number(s): 33.80.Eh, 33.60.Fy, 03.65.Nk

I. INTRODUCTION

Photoionization of core electrons of atoms and molecules is often accompanied by the simultaneous excitation of secondary electrons. In the photoelectron spectrum the results of these shake-up processes manifest themselves as satellites. Theoretically, there can be an infinite number of such satellites. However, only a few will have observable intensities. This phenomena may be substantial in unsaturated molecules. Satellites with intensities up to 25% of that of the primary or the core-hole (CH) line have been observed in N(1s) photoionization of N_2 [1]. Satellite formation is inherently a multielectron process. Hence, a quantitative comparison between theoretical and experimental cross sections for the formation of satellites is important in understanding the many-body nature of the atomic and molecular structure and the photoionization process itself.

A series of satellites, associated with the production of the C(1s) core hole, have been observed [1] in the Al $K\alpha$ x-ray photoionization spectrum of CO. The CH line appears at a binding energy of 296.2 eV. The first and the second satellites (which we designate as $S1$ and $S2$, respectively) appear 8.3 and 14.9 eV above the main line. Later, more elaborate experimental work [2,3] attributed the lowest two satellites to be due to $\pi \rightarrow \pi^*$ transitions. The branching ratios (with respect to the CH line) of $S1$ and $S2$ were observed to behave differently close to the threshold; in $S1$ it increases with decreasing photon energy and in $S2$ it decreases. Detailed configuration-interaction (CI) calculations [4] reveal the existence of two distinct $^2\Sigma^+$ states with the primary configuration

$$(1\sigma)^2(2\sigma)^1(3\sigma)^2(4\sigma)^2(5\sigma)^2(1\pi)^3(2\pi)^1$$

at these binding energies. They differ in their spin symmetry; in $S1$ the π subsystem is spin coupled to give an intermediate triplet, while it is a singlet in $S2$. The different behavior of the branching ratios in light of the fact that both $S1$ and $S2$ arise from the same primary configuration has aroused great theoretical interest in these satellites [5].

Shake-up processes are an indication of the importance of electron-correlation effects in core ionization since it cannot be described by the frozen-core model of the photoionization process. A proper description of the process must include the multielectron effects even in its lowest-order form. At higher photon energies one can calculate the photoionization cross section using the sudden approximation [6,7]. In this limit, the cross section is a function of spectroscopic factors which depend only on the bound-state wave functions of the ion and the neutral molecule; the continuum state associated with the photoelectron plays no crucial role. However, close to the threshold and near resonances, one cannot neglect the scattering states, and the explicit inclusion of them into the theory is necessary.

Incorporation of correlation effects in photoionization can be done at three levels: target relaxation, initial and final bound-state correlation, and interchannel coupling. Unlike valence photoionization, relaxation effects in core ionization of molecules is important [8,9]. This can greatly alter the energy positions and the intensities of resonances. Calculations of Guest *et al.* [4] (and our own calculations) reveal the existence of substantial configuration mixing in the wave functions of the residual ion in satellite channels. This necessitates the use of multiconfiguration ionic states. Relatively little work has been done on the molecular electronic excitation process using multiconfigurational target wave functions [10]. Even fewer use substantial configuration expansions [11–13]. It is the usual practice in calculations with multiconfiguration targets to keep the scattering state orthogonal to the bound molecular orbitals and add polarization terms to the expansion to relax this unphysical orthogonality constraint [10]. This formulation leads to the appearance of spurious singularities in the S matrix, and special averaging techniques are required to extract the physical information [14,15]. The multichannel effects in the CO problem, to our knowledge, have hitherto remained unexplored.

In this paper we develop a computational approach to describe the general photoionization problem (not limited to the core ionization problem) which includes relaxation, multiconfiguration, and multichannel effects, in a multichannel configuration-interaction approximation (MCCI), by combining the CI method and the Schwinger variational principle. At the outset, we use scattering states which are not orthogonal to the bound molecular orbitals. We report the results of a detailed MCCI-Schwinger calculation of the C($1s$) photoionization including the two shake-up satellites $S1$ and $S2$.

The rest of the paper is organized as follows: In Sec. II we develop the theory. Computational details are given in Sec. III. Section IV is devoted to the results and a discussion. Conclusions are found in Sec. V. In the Appendix we construct a mathematical proof to show that the optical potential we used has certain desirable mathematical characteristics which enabled us to use Green's-function techniques.

II. THEORY

The multichannel configuration-interaction wave function of a molecule with an ionized electron is written as

$$\Psi_{\mathrm{MCCI}}=\sum_{i=1}^{N_c}\Phi_i(\chi_i)=\sum_{i=1}^{N_c}\sum_{j=1}^{N_b}C_{ij}\psi_j(\chi_i)\ , \tag{1}$$

where χ_i is the ith channel scattering state, Φ_i represents the configuration-interaction wave function of the residual ion in channel i, and N_c is the number of channels. The notation $\psi_j(\chi_i)$ implies a spin-adapted N-electron configuration state function (CSF), not a simple product of ψ_j and χ_i. Φ_i is expanded in a channel-independent CSF basis $\{\psi_j\}$.

Some of the electronic configurations important for the problem under consideration can have more than two singly occupied orbitals. Such configurations can give more than one CSF which differ in their spin coupling. Using a systematic spin-coupling scheme [16], one can easily construct these CSF's. The equations developed here are very general and do not depend on the particular spin-coupling scheme utilized. Also, the equations are equally valid for a low-spin species (e.g., ionized molecule) as well as a high-spin species (e.g., ionized radical).

Let us designate the total and the z component of spin of a N-electron molecule (or ion) by the quantum numbers S_k and M_k, respectively. Since the Hamiltonian and the physical quantities we are interested in are independent of the spin, without loss of generality we can use the spin eigenfunctions with $M_k=S_k$. In general, the residual ion can have two different total spin values, viz., $S^{\pm}_{N-1}=S_N\pm\frac{1}{2}$ (only S^{+}_{N-1} exists for $S_N=0$). Then an $(N-1)$-electron CSF ψ_q has the form

$$\psi_q=\mathcal{A}\{(\phi_l\phi_l\phi_m\phi_m\cdots\phi_\gamma\phi_\kappa\cdots)\times[\alpha\beta\alpha\beta\cdots\Theta_q(n_q;S^{\pm}_{N-1};M^{\pm}_{N-1}=S^{\pm}_{N-1})]\}\ . \tag{2}$$

Here ϕ_η represents a spatial orbital; α and β represent the usual spin-up and spin-down states of a single electron; and $\Theta_q(n_q;S;M)$ is a spin eigenfunction of n_q electrons, with total and azimuth spin quantum numbers S and M, where n_q is the number of singly occupied orbitals in the CSF. $\mathcal{A}$ is the antisymmetrizer. Then using spin addition and subtraction formulas [16], one obtains the following forms for $\psi_q(\chi_j)$:

$$\psi_q(\chi_j)=\mathcal{A}\{(\phi_l\phi_l\phi_m\phi_m\cdots\phi_\gamma\phi_\kappa\cdots\chi_j)\times[\alpha\beta\alpha\beta\cdots\Theta_q(n_q;S^{-}_{N-1};S^{-}_{N-1})\alpha]\} \tag{3a}$$

or

$$\psi_q(\chi_j)=\frac{1}{\sqrt{2(S_N+1)}}\left(-\mathcal{A}\{(\phi_l\phi_l\phi_m\phi_m\cdots\phi_\gamma\phi_\kappa\cdots\chi_j)[\alpha\beta\alpha\beta\cdots\Theta_q(n_q;S^{+}_{N-1};S^{+}_{N-1}-1)\alpha]\}\right.$$
$$\left.+\sqrt{2S_N+1}\,\mathcal{A}\{(\phi_l\phi_l\phi_m\phi_m\cdots\phi_\gamma\phi_\kappa\cdots\chi_j)[\alpha\beta\alpha\beta\cdots\Theta_q(n_q;S^{+}_{N-1};S^{+}_{N-1})\beta]\}\right)\ . \tag{3b}$$

A priori there is no reason to force orthogonality between χ_i and the spatial molecular orbitals $\{\phi_j\}$ (except to the ones which are doubly occupied in all CSF's) and we do not impose such a condition in general. Nonorthogonality allows more flexibility in χ_i and permits the scattering function to include the functional space spanned by the molecular orbitals. However, when a restricted set of channel state functions are included, unphysical resonances will appear in the scattering solutions unless certain orthogonality constraints are imposed.

The MCCI wave function is required to satisfy the projected Schrödinger equation [17]

$$\left\langle\sum_{i=1}^{N_c}\Phi_i(\delta\chi_i)\,\middle|\,H_N-E\,\middle|\,\Psi_{\mathrm{MCCI}}\right\rangle=0\ , \tag{4}$$

where the electronic Hamiltonian in atomic units is

$$H_N=\sum_{i=1}^{N}f(i)+\sum_{\substack{i,j\\ i>j}}^{N}\frac{1}{r_{ij}} \tag{5}$$

and where N is the number of electrons, with

$$f(i)=-\tfrac{1}{2}\nabla_i^2-\sum_\alpha\frac{Z_\alpha}{r_{i\alpha}}\ . \tag{6}$$

In Eq. (4), $\Phi_i(\delta\chi_i)$ represents all possible variations of $\Phi_i(\chi_i)$ which can be obtained by variations in the scattering orbital χ_i. In order to simplify Eq. (4), it is convenient to introduce the projection operator P, defined by

$$P+\sum_{j=1}^{n}|\phi_j\rangle\langle\phi_j|=1\ , \tag{7}$$

where n is the total number of spatial molecular orbitals used to expand the set of CSF's. Replacing χ_i and $\delta\chi_i$ by

$$P\chi_i+\sum_{j=1}^{n}|\phi_j\rangle\langle\phi_j|\chi_i\rangle$$

and

$$P\delta\chi_i+\sum_{j=1}^{n}|\phi_j\rangle\langle\phi_j|\delta\chi_i\rangle$$

in Eq. (4) and integrating over $N-1$ coordinates, one can reduce Eq. (4) to a set of coupled variational equations for the channel scattering functions (see the Appendix for a proof):

$$\langle\delta\chi_i|[f(i)-E_i]|\chi_i\rangle+\sum_{j=1}^{N_c}\langle\delta\chi_i|U_{ij}|\chi_j\rangle=0\ ,\qquad i=1,2,\ldots,N_c \tag{8}$$

with $E_i=E-\varepsilon_i$, where ε_i is the total energy of the residual ionic state in the ith channel. Then E_i is the asymptotic kinetic energy of the photoelectron in the same channel. U_{ij} is the nonlocal optical potential which has the following form (see the Appendix):

$$\begin{aligned}\langle\delta\chi_i|U_{ij}|\chi_j\rangle=&\sum_{\substack{\alpha,\beta,\gamma,\\ \eta,\kappa,\lambda}}\langle\delta\chi_i|\phi_\alpha\rangle\left\langle\phi_\beta(1)\phi_\gamma(2)\left|\frac{1}{r_{12}}\right|\phi_\eta(1)\phi_\kappa(2)\right\rangle\langle\phi_\lambda|\chi_j\rangle C_{ij}^{\alpha\beta\gamma\eta\kappa\lambda}(1)\\
&+\sum_{\alpha,\beta,\gamma,\eta}\langle\delta\chi_i|\phi_\alpha\rangle\left\langle\phi_\beta(1)\phi_\gamma(2)\left|\frac{1}{r_{12}}\right|\phi_\eta(1)[P\chi_j(2)]\right\rangle C_{ij}^{\alpha\beta\gamma\eta}(2)\\
&+\sum_{\alpha,\beta,\gamma,\eta}\left\langle[P\delta\chi_i(1)]\phi_\alpha(2)\left|\frac{1}{r_{12}}\right|\phi_\beta(1)\phi_\gamma(2)\right\rangle\langle\phi_\eta|\chi_j\rangle C_{ij}^{\alpha\beta\gamma\eta}(3)\\
&+\sum_{\alpha,\beta}\left\langle[P\delta\chi_i(1)]\phi_\alpha(2)\left|\frac{1}{r_{12}}\right|\phi_\beta(1)[P\chi_j(2)]\right\rangle C_{ij}^{\alpha\beta}(4)+\sum_{\alpha,\beta}\left\langle[P\delta\chi_i(1)]\phi_\alpha(2)\left|\frac{1}{r_{12}}\right|[P\chi_j(1)]\phi_\beta(2)\right\rangle C_{ij}^{\alpha\beta}(5)\\
&+\sum_{\alpha,\beta,\gamma,\eta}\langle\delta\chi_i|\phi_\alpha\rangle\langle\phi_\beta(1)|f(1)|\phi_\gamma(1)\rangle\langle\phi_\lambda|\chi_j\rangle C_{ij}^{\alpha\beta\gamma\eta}(6)\\
&+\sum_{\alpha,\beta}\langle\delta\chi_i|\phi_\alpha\rangle\langle\phi_\beta(1)|f(1)|[P\chi_j(1)]\rangle C_{ij}^{\alpha\beta}(7)+\sum_{\alpha,\beta}\langle[P\delta\chi_i(1)]|f(1)|\phi_\alpha(1)\rangle\langle\phi_\beta|\chi_j\rangle C_{ij}^{\alpha\beta}(8)\\
&+\sum_{\alpha}\langle\delta\chi_i|\phi_\alpha\rangle E\langle\phi_\alpha|\chi_j\rangle C_{ij}^{\alpha\beta}(9)+\delta_{ij}\sum_{\alpha}\langle\delta\chi_i|\phi_\alpha\rangle E_i\langle\phi_\alpha|\chi_j\rangle C_{ij}^{\alpha\beta}(10)\ .\end{aligned} \tag{9}$$

The coefficients $C_{ij}^{\alpha\cdots}(m)$ depend on the coefficients C_{ik},C_{jk}, and the electronic configurations used to construct the expansion in Eq. (1).

The potential $\underline{U}$ has no differential operators acting on $\{\chi_i\}$ [18]. All the differential parts are in the first term of Eq. (8). Hence, Eq. (8) is in a suitable form for the application of Green's-function techniques.

Now suppose that we want to force orthogonality between a given channel scattering state and a selected set of molecular orbitals which defines the projection operator q_i:

$$q_i=\sum_{\phi_k\in\text{set }i}|\phi_k\rangle\langle\phi_k|,\quad i=1,2,\ldots,N_c\ . \tag{10}$$

Then the variational equations satisfied by the orthogonal part of the scattering states are [19]

$$\langle(1-q_i)\delta\chi_i|[f(i)-E_i]|(1-q_i)\chi_i\rangle+\sum_{j=1}^{N_c}\langle(1-q_i)\delta\chi_i|U_{ij}|(1-q_k)\chi_j\rangle=0\ ,\qquad i=1,2,\ldots,N_c\ . \tag{11}$$

To construct the Lippmann-Schwinger equation which is equivalent to Eq. (11), we use the channel matrix Phillips-Kleinman pseudopotential [19,20], whose dimensions are N_c by N_c,

$$\underline{V}_Q=\underline{V}-\underline{L}\underline{Q}-\underline{Q}\underline{L}+\underline{Q}\underline{L}\underline{Q}\ , \tag{12}$$

where $\underline{L}$, $\underline{Q}$, and $\underline{V}$ are defined by

$$L_{ij}=\left[-\frac{1}{2}\nabla_i^2-\frac{1}{r}-E_i\right]\delta_{ij}+V_{ij}\ , \tag{13}$$

$$Q_{ij}=q_i\delta_{ij}\ , \tag{14}$$

$$V_{ii}=-\sum_{\alpha}\frac{Z_\alpha}{r_{i\alpha}}+\frac{1}{r}+U_{ii},\quad V_{ij}=+U_{ij}\ . \tag{15}$$

The matrix Lippmann-Schwinger equation [17,21] is then

$$\bar{\chi}=\bar{\chi}^0+\underline{G}_c\underline{V}_Q\bar{\chi}\ , \tag{16}$$

where $\bar{\chi}$ and $\bar{\chi}^0$ are the vectors of the channel scattering states and the channel Coulomb waves. $\underline{G}_c$ is the mul-

tichannel Coulomb Green's matrix defined by

$$(\underline{G}_c)_{ij}=G_c(E_i)\delta_{ij} \ . \tag{17}$$

Although we are interested in photoionization here, the theory described so far is very general and can be used to study electron-molecule collisions as well. The Schwinger variational principle can be utilized to solve Eq. (16) to study photoionization [22]. Let the initial state (i.e., unionized) of the molecule be represented by Ψ_0. In an ideal calculation the final channel wave functions must be orthogonal to Ψ_0 since they represent different stationary states of the same N-electron Hamiltonian. However, because of the approximate nature of the solution, there may be slight nonorthogonality between $\Phi_i(\chi_i)$ and Ψ_0 which can lead to meaningless self-transitions. Thus the self-term has to be subtracted out in defining the transition moment. With the appropriate projection operator, the channel photoionization cross section is proportional to the square of the matrix element:

$$I_i^{L(V)}=\left[\left\langle\Psi_0\left|\sum_{j=1}^{N}\mu_i^{L(V)}(j)\right|\Phi_i(\chi_i)\right\rangle -\left\langle\Psi_0\left|\sum_{j=1}^{N}\mu_i^{L(V)}(j)\right|\Psi_0\right\rangle\langle\Psi_0|\Phi_i(\chi_i)\rangle\right] , \tag{18}$$

where $\mu_i^{L(V)}$ is the one-electron dipole operator; $\mu_i^L(j)=\sqrt{k_i}\,\mathbf{r}_j\cdot\hat{\mathbf{n}}$ in length form and

$$\mu_i^V(j)=(\sqrt{k_i}/\hbar\omega)\nabla_j\cdot\hat{\mathbf{n}}$$

in velocity form, with $\mathbf{k}_i$ representing the momentum of the photoelectron in channel i, $\hat{\mathbf{n}}$ the direction of polarization of the light, and ω the angular frequency of the photon.

The correlated initial-state wave function is expanded in a set of N-electron CSF's which in turn are expanded in a molecular-orbital basis $\{\phi_j'\}$, which is orthonormal to $\{\phi_j\}$. Using the projection operator technique described earlier, one can simplify the channel transition moment to a sum over one-electron integrals:

$$I_i^{L(V)}=\langle R_i^{L(V)}|\chi_i\rangle=\sum_{\alpha,\beta,\gamma}\langle\phi_\alpha'(1)|\mu_i^{L(V)}(1)|\phi_\beta(1)\rangle\langle\phi_\gamma|\chi_i\rangle D_i^{\alpha\beta\gamma}(1)+\sum_{\alpha}\langle\phi_\alpha'(1)|\mu_i^{L(V)}(1)|[P\chi_i(1)]\rangle D_i^{\alpha}(2) \ . \tag{19}$$

Then the double-differential photoionization cross section in length (or velocity) and the mixed form in the body fixed frame is given by [23]

$$\frac{d^2\sigma_i^{L(V)}}{d\Omega_{\hat{\mathbf{k}}_i}d\Omega_{\hat{\mathbf{n}}}}=\frac{4\pi^2\hbar\omega}{c}|I_i^{L(V)}|^2 \ , \tag{20}$$

$$\frac{d^2\sigma_i^{M}}{d\Omega_{\hat{\mathbf{k}}_i}d\Omega_{\hat{\mathbf{n}}}}=\frac{4\pi^2\hbar\omega}{c}\,\mathrm{Re}\{(I_i^L)^*I_i^V\} \ , \tag{21}$$

respectively. The final cross sections are obtained in the usual manner by integrating over all orientations of the molecule in the laboratory frame to give the differential cross section as [24]

$$\frac{d\sigma_i^{L(V,M)}}{d\Omega_{\hat{\mathbf{k}}}}=\frac{\sigma_i^{L(V,M)}}{4\pi}[1+\beta_i^{L(V,M)}P_2(\cos\theta)] \ , \tag{22}$$

where θ is the angle between $\hat{\mathbf{n}}$ and $\hat{\mathbf{k}}$, P_2 is the Legendre polynomial of degree 2, and $\beta_i^{L(V,M)}$ is the photoelectron asymmetry parameter in the length (velocity or mixed) form. The mixed form of the cross section is believed to be more useful than either the usual length or velocity forms of the cross section since the oscillator strength computed in the mixed form satisfies the Thomas-Reiche-Kuhun (TRK) sum rule [25].

III. COMPUTATIONS

The calculations are done in two stages. The first stage involves the determination of $\{\phi_j\}$ and $\{\psi_q\}$, calculation of the coefficients C_{ij} and construction of the potential $\underline{V}_Q$. Calculation Ψ_0 is also done in the first stage. Solution of Eq. (14) and evaluation of photoionization parameters are accomplished in the second stage using well-documented techniques [22].

In principle, any orthonormal molecular-orbital basis can be used to expand the CSF's $\{\psi_q\}$. However, for practical considerations it is desirable to keep N_b to a minimum. To this end, we have used a set of natural orbitals [26] which give a rapidly converging series in Eq. (1). A set of molecular orbitals were generated by performing a restricted open-shell Hartree-Fock (ROHF) calculation on the CH state of CO^+. The natural orbitals were then generated by doing a single-reference singles and doubles (SD) configuration-interaction calculation, using the full set of ROHF orbitals, with the CH configuration as the reference. Gaussian atomic basis sets were used in constructing the molecular orbitals. The results reported here were generated using the standard triple zeta valence plus polarization (TZVP) bases [27]. We have checked the stability of the cross sections and the asymmetry parameters against the changes in basis by repeating the calculation, at a few points, using a much larger (quadruple ζ) Gaussian basis. All the calculations were done at the equilibrium bond length of CO; $R=1.128$ Å.

To construct the CSF basis, we first performed a SD-CI on each channel using the full natural orbital basis (40 functions in TZVP basis). The reference for each channel was chosen to be its primary configuration(s). We have not truncated the molecular-orbital basis, at this stage, since the occupation numbers do not form a reliable criterion when one wants to pick a few prominent configurations. The first few most important CSF's in each channel were included in $\{\psi_q\}$. We have 30 CSF's functions in the set which exploits only 15 molecular orbitals. At present we have included states which have only three or fewer singly occupied orbitals. This is not a

serious limitation especially for the CH and $S1$ states since the most important configurations do not have more than three open orbitals. The spin coupling was accomplished using Yamanouchi-Kotani genealogical spin functions [16]. Table I lists the different types of ψ_q and the corresponding $\psi_q(\chi_i)$ included in our calculations. There, in self-explanatory notation, ϕ_a^α represents a spin orbital with spin α and spatial factor ϕ_a, $\mathcal{A}$ is the antisymmetrizer, and (core) describes the doubly occupied orbital manifold. A limited CI was then performed in ψ_q to determine the coefficients C_{iq} for the residual ionic state in each channel. These coefficients were kept constant during subsequent scattering calculations. We have utilized the GAMESS computer code [28] for all self-consistent field (SCF) and CI calculations.

One needs the potential in the algebraic form depicted in Eq. (9) for the iterative calculations in the second stage. The primary entity needed to construct this operator is

$$\langle \Phi_i(\delta\chi_i)|H_N|\Phi_j(\chi_j)\rangle \ .$$

Here we only outline the philosophy behind the methods we used since the rest is a straightforward exercise in computer programming.

Each SCF is a sum of Slater determinants. Hence a matrix element of the Hamiltonian in the channel basis is a summation of matrix elements over Slater determinants. Since $\{\chi_i\}$ is not orthogonal to $\{\phi_j\}$, Condon-Slater rules [26] are not directly applicable for further reduction of these matrix elements. However, this difficulty can be easily removed by expanding each channel scattering state in the molecular-orbital basis set (used to construct ψ_q) and the part orthogonal to them. Then the matrix elements reduce to a summation over the usual single- and double-electron integrals. We have developed a FORTRAN code to perform the necessary algebraic manipulations and evaluate the coefficients $C_{ij}^{\alpha\cdots}$ using $\{\Phi_i\}$ as the input. With slight modification, the same program was used to calculate the coefficients $D_i^{\alpha\cdots}$ in Eq. (19).

We had to force orthogonality between the channel scattering states and a number of molecular orbitals to avoid spurious resonances. We recognize a singularity in the S matrix as spurious if (a) it is present in a single-channel calculation but is absent in a multichannel calculation or (b) it appears well above the threshold. In single-channel calculations the inclusion of the 4σ orbital leads to such a resonance, in the CH channel around 43.8 eV above threshold and $S2$ right at the threshold. The 5σ molecular orbital creates one 11.8 eV above threshold in the CH channel. A sharp spurious resonance observed in the CH channel at 10.8 eV above threshold and a very broad resonance in $S1$ at 30.5 eV above threshold was due to the $1\pi\pm$ component in the channel scattering state. In multichannel calculations $1\pi\pm$ leads to a broad resonance, at a photon energy of 360 eV, in $S1$ and $S2$ channels and a narrow resonance at 223.0 eV in $S1$. All the results reported here were generated by keeping the channel scattering states orthogonal to 4σ, 5σ, and $1\pi\pm$ orbitals. We must remark here that the exclusion of these orbitals from the channel scattering functions is in agreement with the recently proposed prescription in Ref. [13]. We have checked that the relaxation of this restriction does not have a significant effect either on the cross sections or the asymmetry parameters at photon energies other than where the singularities appear.

The initial-state wave function Ψ_0 was determined as follows: First, a SD-CI calculation was performed on the ground state of CO, using the full set of natural orbitals of CO^+ obtained as described earlier, to determine the important configurations. Then another CI calculation was performed in a truncated CSF basis to obtain the final wave function. This included 85 CSF's which are expanded in 31 natural orbitals. It is not surprising that Ψ_0 needs more CSF's in its expansion to achieve comparable accuracy since the natural orbitals were optimized for the ionic state of CO.

The multichannel Schwinger approach with Padé approximate corrections [21,22] was used in all reported calculations. Explicitly, the variational expression for the channel transition moment was

$$I_i^{L(V)} = \langle R_i^{L(V)}|\chi_i^0\rangle + \sum_{\alpha,\beta}\langle R_i^{L(V)}|\underline{G}_c\underline{V}_Q|\phi_\alpha''\rangle\langle \underline{V}_Q - \underline{V}_Q\underline{G}_c\underline{V}_Q\rangle^{-1} \times \langle \phi_\beta''|\underline{V}_Q|\chi_i^0\rangle \ , \tag{23}$$

where $\{\phi_i''\}$ forms a multichannel scattering basis set and $\langle R_i^{L(V)}|$ is defined in Eq. (19). We have used the total set of natural orbitals, including 1, 3, 4, 5σ, $1\pi\pm$, and δ orbitals, as our scattering basis. There were 16 functions in each σ channel and 7 in each π channel. This represents a substantial reduction of the basis size compared to the Gaussian bases used in previous calculations [5]. Molecular orbitals are more efficient in describing the space around the nuclei than individual Gaussian basis functions. These were sufficient to give an initial guess which converges rapidly on iteration—usually to three to four figures in cross section and asymmetry parameter in three iterations.

All of the integrals in Eq. (19) were evaluated using numerical techniques based on single-center expansions cen-

TABLE I. Forms of $(N-1)$- and the corresponding N-electron CSF's used in our calculations.

Type	ψ_q	$\psi_q(\chi_i)$
1	$\mathcal{A}[(\text{core})\phi_a^\alpha]$	$\mathcal{A}[(\text{core})(\phi_a^\alpha\chi_i^\beta+\chi_i^\alpha\phi_a^\beta)]/\sqrt{2}$
2	$\mathcal{A}[(\text{core})(\phi_a^\alpha\phi_b^\beta\phi_c^\alpha+\phi_b^\alpha\phi_a^\beta\phi_c^\alpha)]/\sqrt{2}$	$\mathcal{A}[(\text{core})(\phi_a^\alpha\phi_b^\beta\phi_c^\alpha\chi_i^\beta+\phi_a^\alpha\phi_b^\beta\chi_i^\alpha\phi_c^\beta+\phi_b^\alpha\phi_a^\beta\phi_c^\alpha\chi_i^\beta+\phi_b^\alpha\phi_a^\beta\chi_i^\alpha\phi_c^\beta)]/2$
3	$\mathcal{A}[(\text{core})(\phi_b^\alpha\phi_a^\beta\phi_c^\alpha-\phi_a^\alpha\phi_b^\beta\phi_c^\alpha-2\phi_a^\alpha\phi_c^\beta\phi_b^\alpha)]/\sqrt{6}$	$\mathcal{A}[(\text{core})(\phi_b^\alpha\phi_a^\beta\phi_c^\alpha\chi_i^\beta+\phi_a^\alpha\phi_b^\beta\chi_i^\alpha\phi_c^\beta-\phi_a^\alpha\phi_b^\beta\phi_c^\alpha\chi_i^\beta-\phi_b^\alpha\phi_a^\beta\chi_i^\alpha\phi_c^\beta-2\phi_a^\alpha\phi_c^\beta\phi_b^\alpha\chi_i^\beta-2\chi_i^\alpha\phi_b^\beta\phi_c^\alpha\phi_a^\beta)]/\sqrt{12}$

tered at the bond midpoint, which has been discussed in detail elsewhere [22,29]. Here we only give a brief account of the parameters used in our calculations. The radial grid had 1696 points and extended to a distance of 100 a.u. The grid points were chosen using a set of well-defined empirical rules [30]. The integration formulas used for radial integrals on this grid were Newton-Cotes-type formulas [29] which allow for the accurate integration of functions which have discontinuities in their slopes, such as those which occur in the integration of Coulomb Green's function and in the integration of $1/r_{12}$.

The partial-wave expansions used in this study were as follows: $l_m = 60$, where l_m is the maximum l included in the expansion of the scattering functions as well as target orbitals at all times; $\lambda_m^{ex} = 60$, where λ_m^{ex} is the maximum l included in the expansion of $1/r_{12}$ in the exchange and $\lambda_m^{st} = 120$ for the static potential terms; and $l_p = 10$, where l_p is the maximum l included in the expansion of the homogeneous solutions $\bar{\chi}^0$.

IV. RESULTS AND DISCUSSION

In Table II we have compared the energies of the residual ionic states calculated with our final CI wave functions with the extended-root-set CI calculations [4] and the experiment results [1]. Our transition energies are in reasonably good agreement with the experiment. It is known [4] that in $S2$, there are correlation contributions coming from configurations which have a larger number of singly occupied orbitals than we have presently included in our expansions. We attribute the relatively larger departure of the transition energy from the experimental value to this. We have used the transition energies shown in Table II as the energy thresholds of the satellites relative to the CH channel in our scattering calculations. As for the ionization threshold of the CH channel, we have used the experimental ionization potential of 296.2 eV.

We have reported the CI coefficients of the primary CSF's in each of the normalized ionic wave functions in Table III. The sum of the squares of the expansion coefficients of the primary CSF's in $S1$ and $S2$ are 0.92 and 0.72, respectively. This gives a measure of the importance of the other configurations in the satellite wave functions. Multiconfigurational effects are somewhat more important in $S2$ than in $S1$.

First, a calculation, at iteration zero, was performed on an evenly spaced photon-energy grid to detect the resonances. Since the spacing of this grid is 0.5 eV, we might not have detected any resonances whose width is less than 0.5 eV. Once the resonances have been isolated, a suitable set of photon energies were determined to do the final iterative calculations.

TABLE II. Comparison of our transition energies with the experiment and extended-root-set CI calculations. The calculated energy of the residual ion in the CH channel reported in Ref. [4] is -101.9899 a.u. Our value is -101.9414 a.u.

Channel	Transition energy (eV)		
	Present	Previous theory[a]	Experiment[b]
CH	0.0	0.0	0.0
$S1$	8.2	8.5	8.3
$S2$	17.5	15.7	14.9

[a]Reference [4].
[b]Reference [1].

A. Core-hole channel

We have plotted the length and velocity forms of the cross section for the σ and π components in single and multichannel calculations leading to the CH state in Figs. 1 and 2, respectively. A strong shape resonance centered at 308.0 eV is observed in the σ cross section. Multichannel effects are virtually absent in this component. Quite prominent multichannel effects are observed in the π component. A Rydberg progression of autoionization peaks is present close to the threshold. In Figs. 3 and 4 we have displayed the asymmetry parameter for the σ and π components. Multichannel effects are less important in determining the asymmetry parameter. Agreement between the length and velocity forms, for both the cross section and the asymmetry parameter, is quite good, except very close to the threshold.

We have compared our total cross sections (in mixed form which satisfies the Thomas-Reiche-Kohn sum rule [25]) and the asymmetry parameters with recent experiment and theoretical calculations in Figs. 5 and 6. The two less intense autoionizing peaks in the π cross section get washed out in the total cross section because of the strong σ resonance. Our results, both cross section and asymmetry parameter, are in good agreement with the recent experimental results of Ref. [33]. Our results closely resemble (except the peak in cross section due to autoionization in the π component in multichannel results) the (single-channel) relaxed core Hartree-Fock calculations of Ref. [9] (which used two separate sets of orbitals, which are orthogonal among themselves but otherwise nonorthogonal, to expand the molecular and the ionic wave functions). This shows that we have successfully retained the orthogonality in the molecular-orbital basis used to expand the wave functions of unionized molecular state and the residual ionic state by representing the initial state by a linear combination of CSF's expanded in relaxed orbitals. Orthogonality among molecular orbitals is a useful feature, especially when one wants to use large CI expansions to accurately account for the correlation effects in the initial as well as the final states.

B. Satellites

In earlier experimental studies of the satellites [1–3], intensities appearing close to the respective thresholds, 304.5 and 311.1 eV, were attributed to be solely due to the $^2\Sigma^+$ states discussed in this paper. However, recent experimental work [33,34] has shown that the photoelectron flux close to these thresholds is partly due to other electronic states (for a discussion on this point, we refer the reader to Ref. [34]). Hence, one must be cautious in comparing our results with the experiment. The cross sections in Ref. [33] are approximately corrected to take into account the effects of the other electronic states.

TABLE III. CI expansion coefficients of the primary CSF's in the normalized residual ion wave functions.

Configuration	CSF type	CH	C_{ij} $S1$	$S2$
$1\sigma^2 2\sigma^1 3\sigma^2 4\sigma^2 5\sigma^2 1\pi^2_- 1\pi^2_+$	1	0.9497	−0.1334	0.0191
$1\sigma^2 2\sigma^1 3\sigma^2 4\sigma^2 5\sigma^2 1\pi^1_- 1\pi^2_+ 2\pi^1_-$	2	0.0015	−0.0283	0.6025
$1\sigma^2 2\sigma^1 3\sigma^2 4\sigma^2 5\sigma^2 1\pi^2_- 1\pi^1_+ 2\pi^1_+$	2	0.0015	−0.0283	0.6025
$1\sigma^2 2\sigma^1 3\sigma^2 4\sigma^2 5\sigma^2 1\pi^1_- 1\pi^2_+ 2\pi^1_-$	3	0.0907	0.6813	0.0321
$1\sigma^2 2\sigma^1 3\sigma^2 4\sigma^2 5\sigma^2 1\pi^2_- 1\pi^1_+ 2\pi^1_+$	3	0.0907	0.6813	0.0321

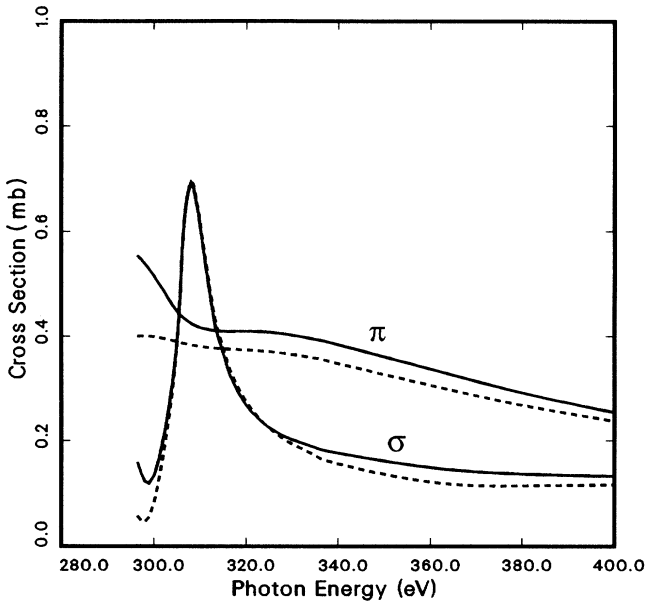

FIG. 1. Present single-channel σ and π cross sections for the CH channel: ——, length form; — — —, velocity form.

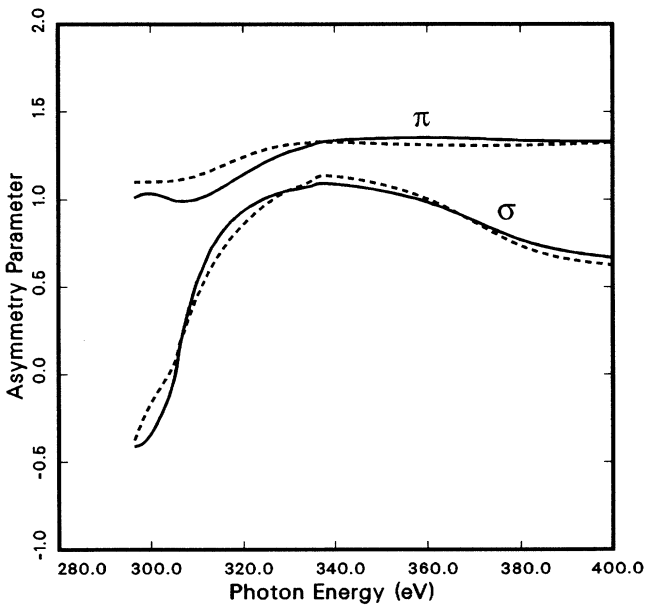

FIG. 3. Present single-channel σ and π asymmetry parameters for the CH channel: ——, length form; — — —, velocity form.

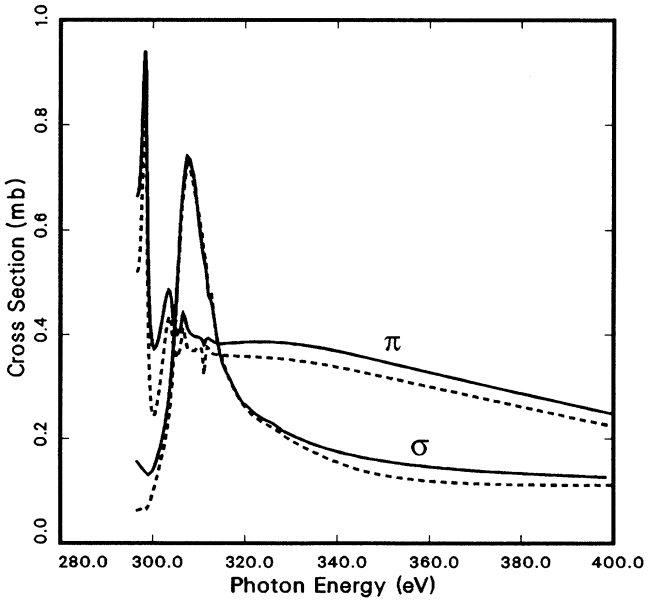

FIG. 2. Present multichannel σ and π cross sections for the CH channel: ——, length form; — — —, velocity form.

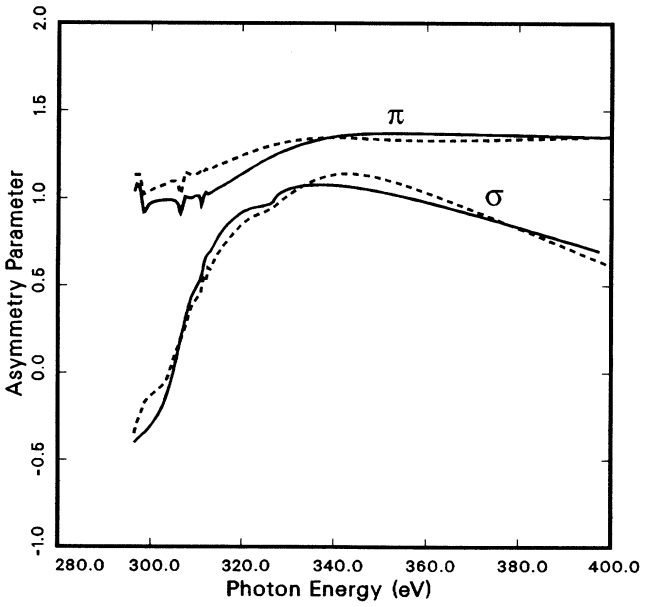

FIG. 4. Present multichannel σ and π asymmetry parameters for the CH channel: ——, length form; — — —, velocity form.

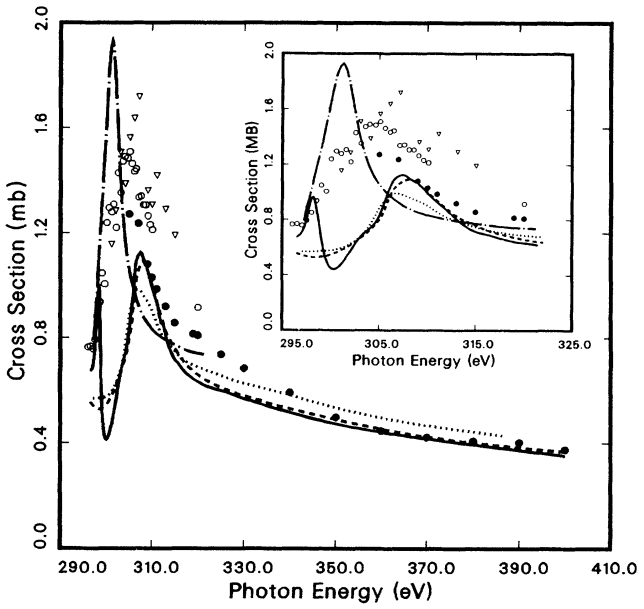

FIG. 5. Comparison of the present CH channel total cross section with previous theory and experiment. Theory: — — —, present single channel; ——, present multichannel; · · · ·, relaxed core Hartree-Fock, Ref. [5]; —·—·—·, frozen-core Hartree-Fock, Ref. [5]. Experiment: ○, Ref. [31]; ▽, Ref. [32]; ●, Ref. [33]. The inset is a closer view of the lower photon-energy part of the same plot.

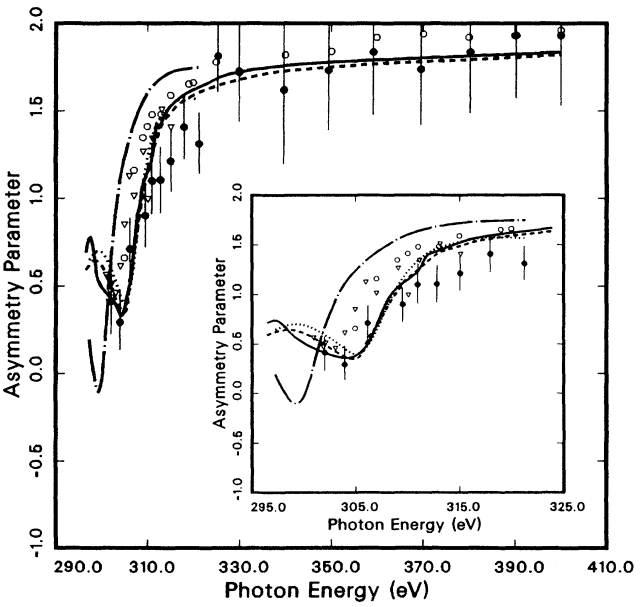

FIG. 6. Comparison of the present CH channel total asymmetry parameter with previous theory and experiment. Theory: — — —, present single channel; ——, present multichannel; · · · ·, relaxed core Hartree-Fock, Ref. [5]; —·—·—·, frozen-core Hartree-Fock, Ref. [5]. Experiment: ▽, Ref. [32]; ●, Ref. [2]; ○, Ref. [33]. The inset is a closer view of the lower photon-energy part of the same plot.

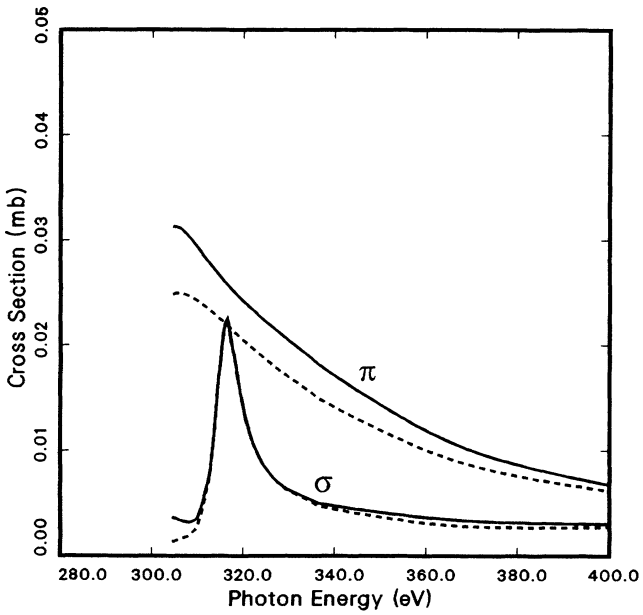

FIG. 7. Present single-channel σ and π cross sections for the $S1$ channel: ——, length form; — — —, velocity form.

In Figs. 7, 8, 9, and 10, we have displayed the length and velocity forms of the cross sections and asymmetry parameters for the σ and π components of $S1$ in single-channel and multichannel calculations. Overall, good agreement is found between length and velocity forms. A broad resonance peak, centered around 316.0 eV, is present in the σ cross section. Strong multichannel effects are apparent in both σ and π components. The σ cross section is strongly enhanced around 308.0 eV by the σ resonance in the CH channel. The shoulder close to 327.0 eV is presumably due to the multichannel coupling

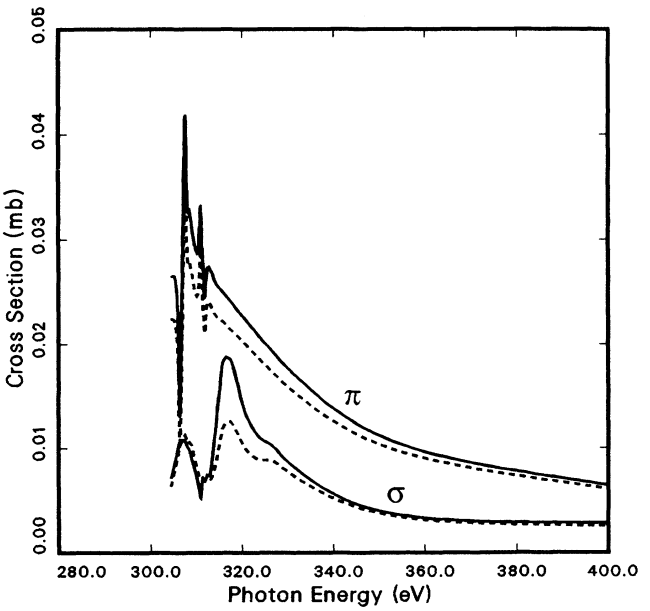

FIG. 8. Present multichannel σ and π cross sections for the $S1$ channel: ——, length form; — — —, velocity form.

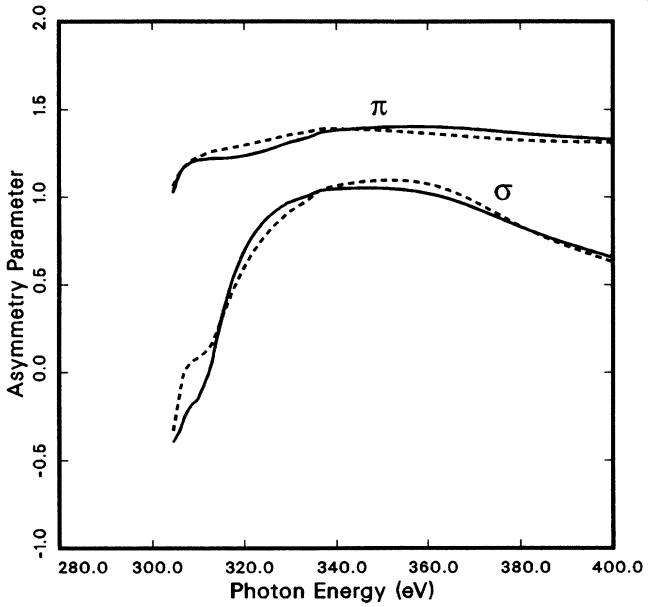

FIG. 9. Present single-channel σ and π asymmetry parameters for the $S1$ channel: ——, length form; — — —, velocity form.

to the resonance in the σ component of $S2$. The multichannel π cross section contains two autoionizing structures below the $S2$ threshold. The σ asymmetry parameter is more influenced by interchannel coupling than the π asymmetry parameter.

We have compared our total cross sections for $S1$ with the experiment and the (single-channel) relaxed core Hartree-Fock (RCHF) calculations, of Ref. [5], in Fig. 11. Our single-channel cross section qualitatively agrees

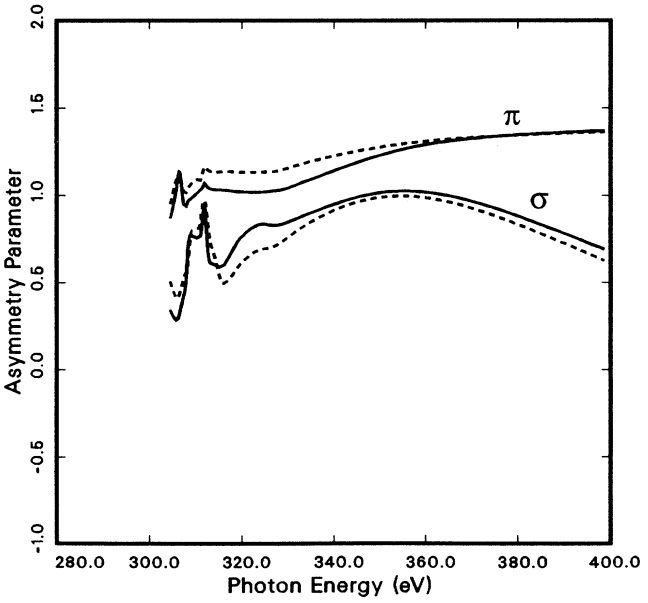

FIG. 10. Present multichannel σ and π asymmetry parameters for the $S1$ channel: ——, length form; — — —, velocity form.

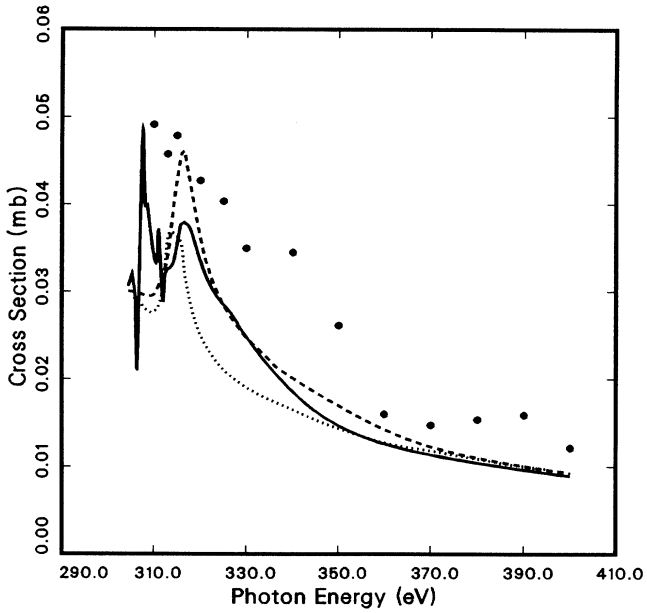

FIG. 11. Comparison of the present $S1$ channel total cross section with previous theory and experiment. Theory: — — —, present single channel; ——, present multichannel; . . . ., relaxed core Hartree-Fock, Ref. [5]. Experiment: ●, Ref. [33].

with RCHF calculations over the whole energy range. The agreement is quantitative at high photon energies. The general trend in theoretical cross sections is well reproduced in the experimental results.

The asymmetry parameter for $S1$ is plotted as a function of photon energy in Fig. 12. There is a distinct dip

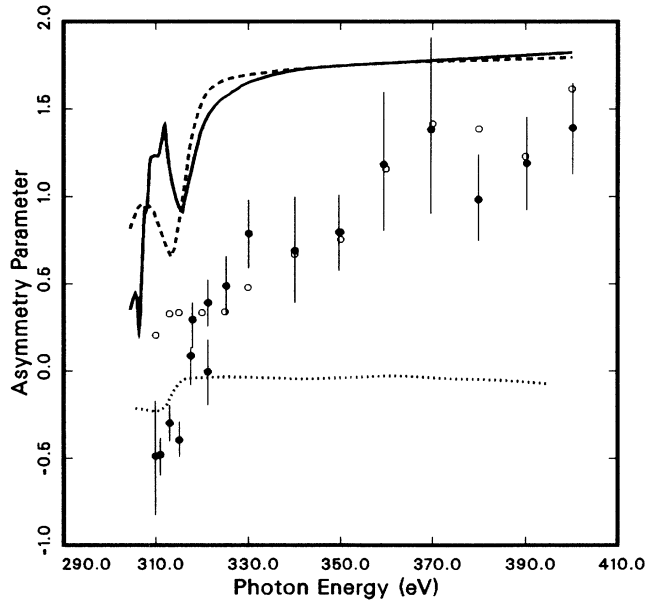

FIG. 12. Comparison of the present $S1$ channel total asymmetry parameter with previous theory and experiment. Theory: — — —, present single channel; ——, present multichannel; . . . ., relaxed core Hartree-Fock, Ref. [5]. Experiment: ●, Ref. [2]; ○, Ref. [33].

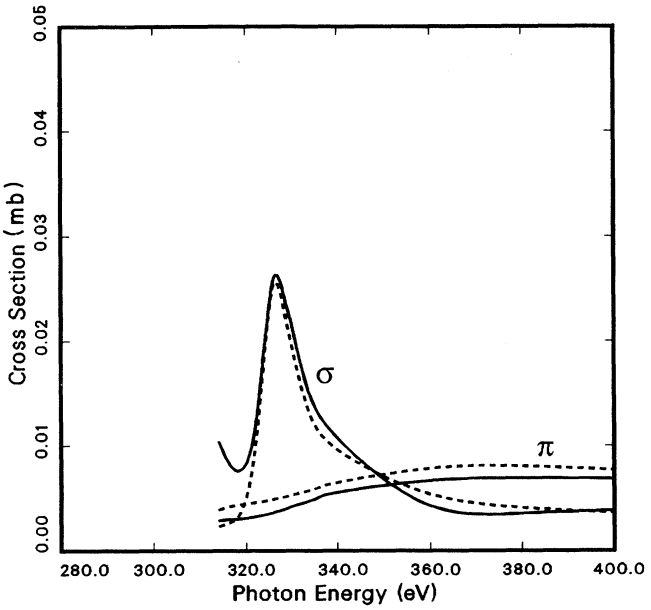

FIG. 13. Present single channel σ and π cross sections for the $S2$ channel: ——, length form; — — —, velocity form.

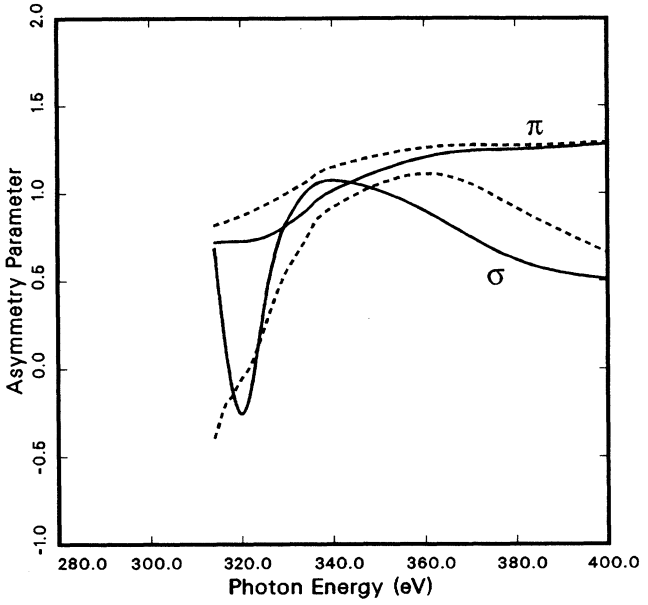

FIG. 15. Present single-channel σ and π asymmetry parameters for the $S2$ channel: ——, length form; — — —, velocity form.

around 314.0 eV in single-channel calculations. Channel coupling shifts this minimum to a higher photon energy and introduces a narrow dip around 306.0 eV. Our results reproduce the experimental trend well. We attribute the differences between our results and RCHF results to the inclusion of multiconfiguration effects in the present calculation.

Figures 13, 14, 15, and 16 give the length and velocity cross sections and asymmetry parameters for different components of $S2$. The agreement between length and velocity forms is quite good except very close to the threshold. The large discrepancy in length and velocity asymmetry parameters, close to the threshold, in the single-channel σ component and the absence of it in the multichannel results show the crucial role played by correlation in determining the asymmetry parameter at lower photon energies. A resonance peak centered at 326.0 eV is present in both single-channel and multichannel σ cross sections.

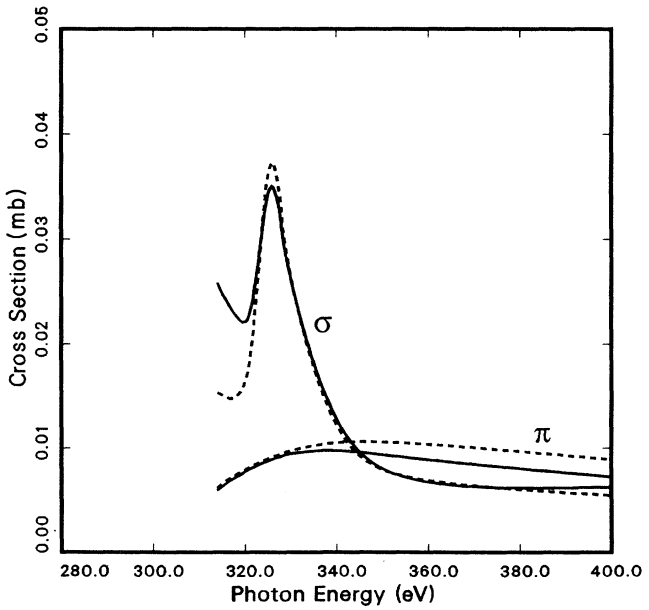

FIG. 14. Present multichannel σ and π cross sections for the $S2$ channel: ——, length form; — — —, velocity form.

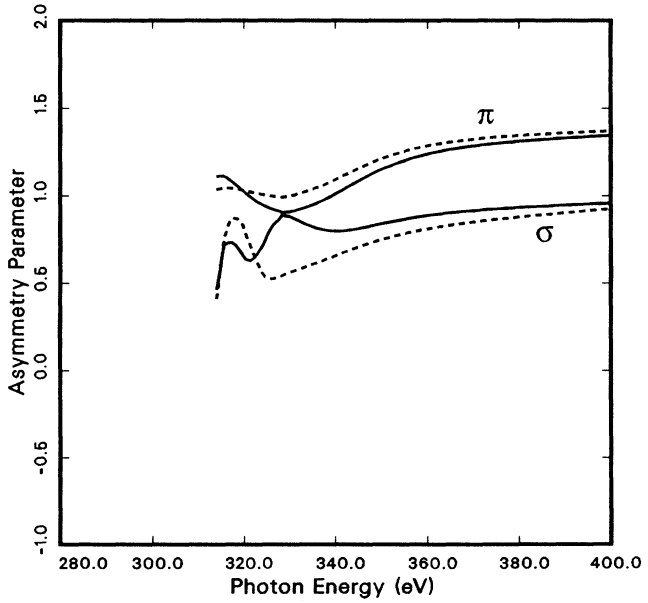

FIG. 16. Present multichannel σ and π asymmetry parameters for the $S2$ channel: ——, length form; — — —, velocity form.

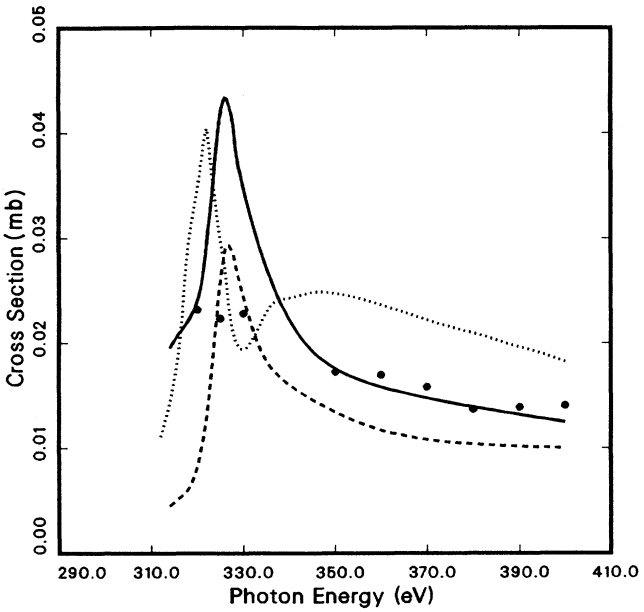

FIG. 17. Comparison of the present $S2$ channel total cross section with previous theory and experiment. Theory: — — —, present single channel; ——, present multichannel; · · · ·, relaxed core Hartree-Fock, Ref. [5]. Experiment ●, Ref. [33].

Total cross sections of the present calculations for $S2$ are compared with the RCHF and experimental results in Fig. 17. Comparison of single-channel results with multichannel calculations reveals that channel coupling is important in determining the cross section in $S2$ not only close to the threshold but also at higher photon energies. Our multichannel results agree well with the experiment at higher energies. Experimental results show no sign of a resonance peak, which is also present in RCHF results, at lower energies.

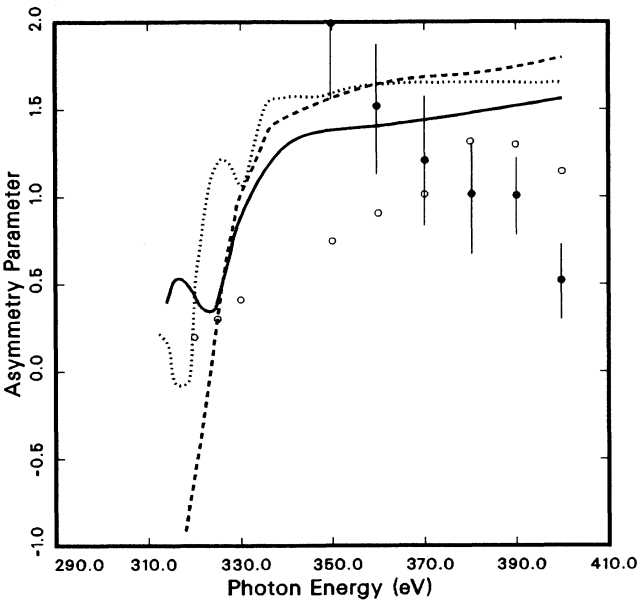

FIG. 18. Comparison of the present $S2$ channel total asymmetry parameter with previous theory and experiment. Theory: — — —, present single channel; ——, present multichannel; . . . ., relaxed core Hartree-Fock, Ref. [5]. Experiment: ●, Ref. [2]; ○, Ref. [33].

We have displayed the asymmetry parameter of $S2$ in Fig. 18. Multichannel results show a maximum and a minimum at 317.5 and 324.0 eV, respectively. Single-channel results deviate from coupled-channel calculations at low photon energy and lead to unphysical values (i.e., negative differential cross sections) near threshold. Such behavior is possible in the mixed form of the cross section (hence, asymmetry parameter) when there is a significant phase difference between the length and velocity forms of the dipole matrix elements used to evaluate Eq. (21). As can be seen in Fig. 15, the length and velocity asymmetry parameters in the σ symmetry have very different near-threshold behavior for the single-channel results leading to the $S2$ state. This again points to the high level of correlation effects in $S2$. The general trend of the experimental results of Hemmers and Becker is reproduced by our multichannel results.

V. CONCLUSIONS

Satellite formation in photoionization is inherently a many-electron phenomenon. Any theory which describes this process must include electron-correlation effects even in zeroth order. Here we have developed such an approach which includes relaxation; configuration interaction, in the initial molecular state as well as the residual ionic state; and multichannel effects in photoionization of molecules (electron-molecule collisions as well), both high spin and low spin. We have rigorously proven that the variational equation for the system wave function (within MCCI approximation) can be reduced to a set of equations for the channel scattering states which is amenable to Green's-function techniques. The solution of these equations, for the case of photoionization, has been done using the Schwinger variational principle. We have demonstrated the feasibility of the theory by applying it to the C($1s$) core-hole production and the associated satellite formation process.

In the core-hole channel, strong autoionizing resonances are observed in the π cross section to the threshold. Multichannel effects are less important in the σ-cross section. The agreement between theory and experiment (both cross section and asymmetry parameter) is very good at higher photon energies. The discrepancies close to the threshold may be attributed to polarization effects.

Multichannel effects are more important in describing the satellites than in the core-hole channel. In $S1$, channel coupling strongly modifies both σ as well as π cross sections close to threshold. The σ asymmetry parameter is also strongly influenced. In $S2$, channel coupling enhances the cross section, in both components, throughout the energy range studied. The general experimental trends are well reproduced by our multichannel results. To make a more reliable judgment on the agreement between experiment and theory for the satellites, one needs highly resolved spectra which can isolate the intensity due to $^2\Sigma^+$ components. Also, the calculations should include CSF's with more unpaired electrons in the

wave functions of the molecule and the residual ion than was possible in this study. Work is under way to generalize our potential generation programs to achieve this goal. Additionally, the calculations should include the channels leading to the other shake-up channels which are open at the energies considered here.

ACKNOWLEDGMENTS

This material is based on work supported in part by the National Science Foundation under Grant No. CHE-83-51414 and in part by the Robert A. Welch Foundation (Houston, TX) under Grant No. A-1020. Support from the Alfred P. Sloan Foundation and from the Camille and Henry Dreyfus Foundation is also gratefully acknowledged. Computations for this work were carried out in part at the Texas A&M Supercomputer Center, the Pittsburgh Supercomputing Center, and on the Department of Chemistry FPS 522 EA computer, which was funded in part by an NFS instrumentation grant.

APPENDIX

The first step in the solution of Eq. (4) is the reduction of it into the set of coupled equations (8). The optical potential $\underline{U}$ in Eq. (8) does not have terms which lead to differentiation of the channel scattering states [18]. Hence, Eq. (8) is in a suitable form for the application of usual Green's-function techniques. Here we construct a proof to show that the variational equation satisfied by the multichannel configuration-interaction wave function of the ionized molecule can always be reduced to the set of equations (8) with the optical potential having the form depicted in Eq. (9).

In the proof, we only assume the expandability of the spin eigenfunctions in primitive spin functions [16] which is true for any spin eigenfunction irrespective of the construction scheme. Hence the equations derived are independent of the spin-coupling scheme.

Expand Θ_q in Eq. (2) in primitive spin functions. Then ψ_q becomes a sum of Slater determinants:

$$\psi_q = \sum_{k=1}^{n_q} d_{qk}\mathcal{A}[D_k^q] , \tag{A1}$$

where D_k^q represents an ordered spin-orbital product where the spin orbitals are arranged in increasing order of the orbital index. Then the orthonormality of $\{\Phi_i\}$ gives.

$$\begin{aligned}\langle\Phi_i|\Phi_j\rangle &= \sum_{q_1,q_2=1}^{N_b} C_{iq_1}^* C_{jq_2}\langle\psi_{q_1}|\psi_{q_2}\rangle \\ &= \sum_{q_1,q_2=1}^{N_b}\sum_{k_1=1}^{n_{q_1}}\sum_{k_2=1}^{n_{q_2}} C_{iq_1}^* d_{q_1k_1}^* C_{jq_2} d_{q_2k_2} \\ &\quad\times\delta_{0n(q_1k_1;q_2k_2)}=\delta_{ij} ,\end{aligned} \tag{A2}$$

where $n(q_1k_1;q_2k_2)$ is the number of spin orbitals by which the sets of spin orbitals in $D_{k_1}^{q_1}$ and $D_{k_2}^{q_2}$ differ.

Using Condon-Slater rules [26] to reduce the Hamiltonian matrix element between any two determinants and using the fact that $\{\Phi_i\}$ are eigenfunctions of H_{N-1}, we obtain

$$\begin{aligned}&\langle\Phi_i|H_{N-1}|\Phi_j\rangle \\ &= \sum_{q_1,q_2=1}^{N_b}\sum_{k_1=1}^{n_{q_1}}\sum_{k_2=1}^{n_{q_2}} C_{iq_1}^* d_{q_1k_1}^* C_{jq_2} d_{q_2k_2} \\ &\quad\times\Bigg[\Bigg[\sum_{\varphi_\gamma\in\omega(q_1k_1)}\langle\varphi_\gamma|f|\varphi_\gamma\rangle+\tfrac{1}{2}\sum_{\varphi_{\gamma,\delta}\in\omega(q_1k_1)}\langle\varphi_\gamma\varphi_\delta\|\varphi_\gamma\varphi_\delta\rangle\Bigg]\delta_{0n(q_1k_1;q_2k_2)} \\ &\quad+\Bigg[\langle\varphi_\eta|f|\varphi_\lambda\rangle+\sum_{\varphi_\gamma\in\omega(q_1k_1)}\langle\varphi_\gamma\varphi_\eta\|\varphi_\gamma\varphi_\lambda\rangle\Bigg](-1)^{n_p(q_1k_1;q_2k_2)}\delta_{1n(q_1k_1;q_2k_2)} \\ &\quad+\langle\varphi_\mu\varphi_\eta\|\varphi_\nu\varphi_\lambda\rangle(-1)^{n_p(q_1k_1;q_2k_2)}\delta_{2n(q_1k_1;q_2k_2)}\Bigg]=\varepsilon_i\delta_{ij} ,\end{aligned} \tag{A3}$$

where $\omega(q_1k_1)$ is the set of spin orbitals in the product $D_{k_1}^{q_1}$, $n_p(q_1k_1;q_2k_2)$ is the number of permutations performed on $D_{k_1}^{q_1}$ to bring the difference between the ordered products $D_{k_q}^{q_1}$ and $D_{k_2}^{q_2}$ to a minimum, $(\varphi_\mu,\varphi_\eta)$ and $(\varphi_\nu,\varphi_\lambda)$ are the spin orbitals by which the sets of spin orbitals in $D_{k_1}^{q_1}$ and $D_{k_2}^{q_2}$ differ, and

$$\langle\varphi_a\varphi_b\|\varphi_c\varphi_d\rangle=\left\langle\varphi_a(1)\varphi_b(2)\left|\frac{1}{r_{12}}\right|\varphi_c(1)\varphi_d(2)\right\rangle-\left\langle\varphi_a(1)\varphi_b(2)\left|\frac{1}{r_{12}}\right|\varphi_c(2)\varphi_d(1)\right\rangle . \tag{A4}$$

It is convenient to divide the problem into three separate cases: case 1, only the ionic states with spin S^- are included; case 2, only the ionic states with spin S^+ are included; and case 3, the most general case, where both spin states are included in the calculation.

Case 1. We expand the right-hand side of Eq. (3a) in Slater determinants:

$$\psi_q(\chi_j)=\sum_{k=1}^{n_q} d_{qk}\mathcal{A}[D_k^q(\chi_j\alpha)] \ . \tag{A5}$$

Now the decomposition of χ_j into orthogonal and nonorthogonal parts gives

$$\Phi_j(\chi_j)=\sum_{q_2=1}^{N_b}\sum_{k_2=1}^{n_{q_2}} C_{jq_2}d_{q_2k_2}\left[\mathcal{A}[D_{k_2}^{q_2}(P\chi_j\alpha)]+\sum_{l=1}^{n}\mathcal{A}[D_{k_2}^{q_2}(\phi_l\alpha)]\langle\phi_l|\chi_j\rangle\right] . \tag{A6}$$

Then

$$\begin{aligned}
&\langle\Phi_i(\delta\chi_i)|H_N-E|\Phi_j(\chi_j)\rangle \\
&\quad=\sum_{q_1,q_2=1}^{N_b}\sum_{k_1=1}^{n_{q_1}}\sum_{k_2=1}^{n_{q_2}} C_{iq_1}^{*}d_{q_1k_1}^{*}C_{jq_2}d_{q_2k_2} \\
&\qquad\times\Bigg[\langle\mathcal{A}[D_{k_1}^{q_1}(P\delta\chi_i\alpha)]|H_N-E|\mathcal{A}[D_{k_2}^{q_2}(P\chi_j\alpha)]\rangle \\
&\qquad\quad+\sum_{l,m=1}^{n}\langle\delta\chi_i|\phi_l\rangle\langle\mathcal{A}[D_{k_1}^{q_1}(\phi_l\alpha)]|H_N-E|\mathcal{A}[D_{k_2}^{q_2}(\varphi_m\alpha)]\rangle\langle\phi_m|\chi_j\rangle \\
&\qquad\quad+\sum_{l=1}^{n}\langle\delta\chi_i|\phi_l\rangle\langle\mathcal{A}[D_{k_1}^{q_1}(\phi_l\alpha)]|H_N|\mathcal{A}[D_{k_2}^{q_2}(P\chi_j\alpha)]\rangle \\
&\qquad\quad+\sum_{m=1}^{n}\langle\mathcal{A}[D_{k_1}^{q_1}(P\delta\chi_i\alpha)]|H_N|\mathcal{A}[D_{k_2}^{q_2}(\phi_m\alpha)]\rangle\langle\phi_m|\chi_j\rangle\Bigg] .
\end{aligned} \tag{A7}$$

In deriving Eq. (A7), we have used the fact that

$$\langle\mathcal{A}[D_{k_1}^{q_1}(P\delta\chi_j\alpha)]|\mathcal{A}[D_{k_2}^{q_2}(\phi_m\alpha)]\rangle=\langle\mathcal{A}[D_{k_1}^{q_1}(\phi_l\alpha)]|\mathcal{A}[D_{k_2}^{q_2}(P\chi_j\alpha)]\rangle=0 \ . \tag{A8}$$

Note that the last three terms of Eq. (A7) involve orthogonal orbitals and hence Condon-Slater rules can be used to reduce the matrix elements over N-electron functions into one- and two-electron integrals. Likewise, one can reduce the first term into constituent integrals by assuming the orbitals $(P\delta\chi_i\alpha)$ and $(P\chi_j\alpha)$ to be equal but not normalized, i.e., $\langle P\delta\chi_i\alpha|P\chi_j\alpha\rangle\neq1$, and applying the Condon-Slater rules.

Observation reveals that, in their most general form, there can be only 13 types of matrix elements in the right-hand side of Eq. (A7). This includes (with the spin integration done) all the terms listed in Eq. (9), except the last term, $\langle P\delta\chi_i|f|P\chi_j\rangle$, $E\langle P\delta\chi_i|P\chi_j\rangle$, $\langle\varphi_a|f|\varphi_b\rangle\langle P\delta\chi_i|P\chi_j\rangle$, and

$$\left\langle\varphi_a\varphi_b\left|\frac{1}{r_{12}}\right|\varphi_c\varphi_d\right\rangle\langle P\delta\chi_i|P\chi_j\rangle \ .$$

These terms originate in the first term of (A7). Reducing this term and regrouping the one- and two-electron integrals using Eqs. (A2) and (A3), we obtain

$$\begin{aligned}
&\langle\mathcal{A}[D_{k_1}^{q_1}(P\delta\chi_i\alpha)]|H_N-E|\mathcal{A}[D_{k_2}^{q_2}(P\chi_j\alpha)]\rangle \\
&\quad=\langle P\delta\chi_i|f|P\chi_j\rangle\delta_{ij}+(\varepsilon_i-E)\langle P\delta\chi_i|P\chi_j\rangle\delta_{ij} \\
&\qquad+\sum_{q_1,q_2=1}^{N_b}\sum_{k_1=1}^{n_{q_1}}\sum_{k_2=1}^{n_{q_2}} C_{iq_1}^{*}d_{q_1k_1}^{*}C_{jq_2}d_{q_2k_2}(-1)^{n_p(q_1k_1;q_2k_2)} \\
&\qquad\quad\times\left[\tfrac{1}{2}\sum_{\varphi_\gamma\in\omega(q_1k_1)}\langle\varphi_\gamma(P\delta\chi_i\alpha)\|\varphi_\gamma(P\chi_j\alpha)\rangle\delta_{0n(q_1k_1;q_2k_2)}+\langle\varphi_\eta(P\delta\chi_i\alpha)\|\varphi_\lambda(P\chi_j\alpha)\rangle\delta_{1n(q_1k_1;q_2k_2)}\right] .
\end{aligned} \tag{A9}$$

Subcase 1: $i\neq j$. From Eq. (A9) it is clear that the terms containing matrix elements of the form $\langle P\delta\chi_i|f|P\chi_j\rangle$ and $\langle P\delta\chi_i|P\chi_j\rangle$ disappear in this case. Hence, the form of the potential depicted in Eq. (9) is certainly true for this case with

$$\langle \Phi_i(\delta\chi_i)|H_N-E|\Phi_j(\chi_j)\rangle=\langle \delta\chi_i|U_{ij}|\chi_j\rangle \ . \tag{A10}$$

Subcase 2: $i=j$. Expanding P using Eq. (7), one obtains for the first two terms of (A9):

$$\begin{aligned}\langle P\delta\chi_i|f|P\chi_i\rangle+[\varepsilon_i-E]\langle P\delta\chi_i|P\chi_i\rangle&=\langle P\delta\chi_i|f-E_i|P\chi_i\rangle\\&=\langle \delta\chi_i|f-E_i|\chi_i\rangle+\sum_{l,m=1}^{n}\langle \delta\chi_i|\phi_l\rangle\langle\phi_l|f|\phi_m\rangle\langle\phi_m|\chi_i\rangle\\&\quad+\sum_{l=1}^{n}\langle \delta\chi_i|\phi_l\rangle\langle\phi_l|f|P\chi_i\rangle+\sum_{m=1}^{n}\langle P\delta\chi_i|f|\phi_m\rangle\langle\phi_m|\chi_i\rangle\\&\quad+\sum_{l=1}^{n}\langle \delta\chi_i|\phi_l\rangle E_i\langle\phi_l|\chi_i\rangle \ .\end{aligned} \tag{A11}$$

Equations (A7), (A9), and (A11) reveal that when $i=j$, the potential has the form stated in Eq. (9) with

$$\begin{aligned}&\langle \Phi_i(\delta\chi_i)|H_N-E|\Phi_i(\chi_i)\rangle\\&\quad=\langle \delta\chi_i|f-E_i|\chi_i\rangle+\langle \delta\chi_i|U_{ii}|\chi_i\rangle \ .\end{aligned} \tag{A12}$$

This concludes the proof for case 1. To avoid writing down, essentially the same, lengthy algebraic equations, we only outline the proofs for the other two cases. Working out the exact expressions is left for the reader as a simple exercise in algebra.

Case 2. We rewrite Eq. (3b), in self-explanatory notation, as follows:

$$\psi_q(\chi_j)=(-X_j^q+\sqrt{2S_N+1}\,Y_j^q)/\sqrt{2(S_N+1)} \ . \tag{A13}$$

The proof, in this case, follows the same steps as above once you realize that (a) $\langle P\delta\chi_i|P\chi_j\rangle$ appears only in terms $\langle X_{q_1}^i|H_N-E|X_{q_2}^j\rangle$ and $\langle Y_{q_1}^i|H_N-E|Y_{q_2}^j\rangle$ because spin integration forbids such terms in $\langle X_{q_1}^i|H_N-E|Y_{q_2}^j\rangle$ and $\langle Y_{q_1}^i|H_N-E|X_{q_2}^j\rangle$, and (b) $\langle \Phi_i|H_{N-1}|\Phi_j\rangle$ is independent of M_{N-1}^+.

Case 3. In this case the matrix elements are

$$\langle \Phi_i(\delta\chi_i)|H_N-E|\Phi_j(\chi_j)\rangle \ ,$$

where one channel, say, i, involves spin S^- and the other, channel j, involves S^+ ionic states. Here, $\langle P\delta\chi_i|P\chi_j\rangle$ appears only in terms

$$\langle \psi_{q_1}(\delta\chi_i)|H_N-E|X_{q_2}^j\rangle \ .$$

The proof can be worked out as above when you realize that fact that

$$\langle \Phi_i|\Phi_j\rangle=\langle \Phi_i|H_{N-1}|\Phi_j\rangle=0$$

irrespective of the azimuthal spin quantum numbers associated with Φ_i and Φ_j since they have different total spin quantum numbers. Hence we have shown that in general one can reduce Eq. (4) to a set of equations (8) for the channel scattering functions with the optical potential given by Eq. (9).

[1] U. Gelius, J. Electron. Spectrosc. Relat. Phenom. **5**, 985 (1974).

[2] A. Reimer, J. Schirmer, J. Feldhaus, A. M. Bradshaw, U. Becker, H. G. Kerkhoff, B. Langer, D. Szostak, R. Wehlitz, and W. Braun, Phys. Rev. Lett. **57**, 1707 (1986).

[3] L. Ungier and T. D. Thomas, Phys. Rev. Lett. **53**, 435 (1984).

[4] M. F. Guest, W. R. Rodwell, T. Darko, I. H. Hiller, and J. Kendrick, J. Chem. Phys. **66**, 5447 (1977).

[5] J. Schirmer, M. Braunstein, and V. McKoy, Phys. Rev. A **44**, 5762 (1991).

[6] T. A. Carlson and M. O. Krause, Phys. Rev. **140**, 1057 (1965).

[7] T. Åberg, Phys. Rev. **156**, 35 (1967).

[8] D. L. Lynch and V. McKoy, Phys. Rev. A **30**, 1561 (1984).

[9] J. Schirmer, M. Braunstein, and V. McKoy, Phys. Rev. A **41**, 283 (1990).

[10] L. A. Collins and B. I. Schneider, in *Proceedings of the Eleventh International Conference on the Physics of Electronic and Atomic Collisions,* edited by H. Gilbody, W. Newell, F. Read, and A. Smith (North-Holland, New York, 1987).

[11] S. E. Branchett and J. Tennyson, Phys. Rev. Lett. **64**, 2889 (1990).

[12] A. E. Orel, T. N. Rescigno, and B. H. Lengsfield, Phys. Rev. A **42**, 5292 (1990).

[13] B. H. Lengsfield III and T . N. Rescigno, Phys. Rev. A **44**, 2913 (1991).

[14] P. G. Burke, K. A. Berrington, and C. V. Sukumar, J. Phys. B **14**, 289 (1981).

[15] H. A. Slim and A. T. Stelbovics, J. Phys. B **20**, L211 (1987).

[16] Ruben Paunz, *Spin Eigenfunctions: Construction and Use* (Plenum, New York, 1979).

[17] R. K. Nesbet, *Variational Methods in Electron-Atom Scattering Theory* (Plenum, New York, 1980), p. 9.

[18] Note that the operator f is Hermitian; hence,

$$\langle \phi_\beta(1)|f(1)|[P\chi_j(1)]\rangle=\langle [f(1)\phi_\beta(1)]|[P\chi_j(1)]\rangle \ .$$

[19] J. D. Weeks, A. Hazi, and S. A. Rice, *Advances in Chemical Physics* (Interscience, New York, 1969), Vol. XVI, p. 283.

[20] B. Basden and R. R. Lucchese, Phys. Rev. A **37**, 89 (1988).

[21] R. R. Lucchese, Phys. Rev. A **33**, 1626 (1986).

[22] R. R. Lucchese, K. Takatsuka, and V. McKoy, Phys. Rep. **131**, 148 (1986).

[23] A. E. Hansen, Mol. Phys. **13**, 425 (1967).
[24] J. C. Tuly, R. S. Berry, and B. J. Dalton, Phys. Rev. **176**, 95 (1968).
[25] A. E. Hansen and T. D. Bouman, Chem. Phys. Lett. **45**, 326 (1977).
[26] A. Zabo and N. S. Ostlund, *Modern Quantum Chemistry* (McGraw-Hill, New York, 1982), pp. 70 and 252.
[27] T. H. Dunning, Jr., J. Chem. Phys. **55**, 716 (1971); A. D. McLean and G. S. Chandler, *ibid.* **72**, 5639 (1980).
[28] M. F. Guest and J. Kendrick, GAMESS User's Manual, SERC Daresbury Laboratory, CCP1/86/1, 1986: M. Dupuis, D. Spangler, and J. Wendoloski, NRCC Software Catalog, Vol. 1, Program No. QG01 (GAMESS), 1980; M. F. Guest, R. J. Harrison, J. H. van Lenthe, and C. L. H. van Corler, Theor. Chim. Acta. **71**, 117 (1987).
[29] B. Basden and R. R. Lucchese, J. Comput. Phys. **77**, 524 (1988).
[30] R. R. Lucchese (unpublished).
[31] R. B. Kay, Ph. E. Van der Leeuw, and M. J. Van der Wiel, J. Phys. B **10**, 2513 (1977).
[32] C. M. Truesdale, S. H. Southworth, P. H. Kobrin, U. Becker, D. W. Lindle, H. G. Kerkhof, and D. A. Shirley, Phys. Rev. Lett. **50**, 1265 (1983); C. M. Truesdale, D. W. Lindle, P. H. Kobrin, U. Becker, H. G. Kerkhoff, P. A. Heimann, T. A. Ferret, and D. A. Shirley, J. Chem. Phys. **80**, 2319 (1984).
[33] O. Hemmers and U. Becker (private communication).
[34] L. J. Medhurst, Ph.D thesis, University of California, Berkeley, 1991: Lawrence Berkeley Laboratory Publication No. LBL-31466, Berkeley, CA 94720.